applied sciences

MDPI

Article

Experimental and Numerical Simulations on the Mechanical Characteristics of Soil–Rock Mixture in Uniaxial Compression

Zhenping Zhang [1,2], Xiaodong Fu [2,3,*], Qian Sheng [2,3], Shuo Wang [1] and Yuwei Fang [4]

[1] School of Architecture and Civil Engineering, Shenyang University of Technology, Shenyang 110870, China; zhangzp21@sut.edu.cn (Z.Z.)
[2] State Key Laboratory of Geomechanics and Geotechnical Engineering, Institute of Rock and Soil Mechanics, Chinese Academy of Sciences, Wuhan 430071, China
[3] School of Engineering Science, University of Chinese Academy of Sciences, Beijing 100049, China
[4] Yunnan Institute of Transport Planning and Design Co., Ltd., Kunming 650200, China
* Correspondence: xdfu@whrsm.ac.cn

Abstract: Soil–rock mixture is a common geo-material found in natural deposit slopes and various constructions, such as tunnels, hydropower stations, and subgrades. The complex mechanical characteristics of soil–rock mixture arise from its multi-phase compositions and cooperative interactions. This paper investigated the mechanical properties of soil–rock mixture, focusing on the influence of rock content, and soil–rock interface strength was discussed. Specimens with varying rock contents were subjected to uniaxial compression tests. The results indicated that rock content, as a key structural parameter, significantly controls the crack propagation trends. As rock content increases, the initial structure of the soil matrix is damaged, leading to the formation of a weak-strength soil–rock interface. The failure mode transitions from longitudinal cracking to multiple shear fractures. To analyze the strength of the soil–rock interface from a mesoscopic perspective, simulations of soil–rock mixture specimens with irregular rock blocks were conducted using the particle discrete element method (PDEM). At the meso-scale, the specimen with 30% rock content exhibited a complex particle displacement distribution, with differences in the direction and magnitude of displacement between soil and rock particles being critical to the failure modes of the specimen. As the soil–rock interface strength increased from 0.1 to 0.9, the distribution of force chains within the specimen shifted from a centralized to a more uniform distribution, and the thickness of force chains became increasingly uniform. The strength responses of the soil–rock mixture under uniaxial compression condition were discussed, revealing that the uniaxial compression strength (UCS) of soil–rock mixture decreases exponentially with increasing rock content. An estimation formula was developed to characterize the UCS of soil–rock mixture in relation to rock content and interface strength. The findings from both the experiments and simulations can provide valuable insights for evaluating the stability of deposit slopes and other constructions involving soil–rock mixture.

Keywords: soil–rock mixture; uniaxial compression test; uniaxial compressive strength; irregular rock block; failure mechanism

Citation: Zhang, Z.; Fu, X.; Sheng, Q.; Wang, S.; Fang, Y. Experimental and Numerical Simulations on the Mechanical Characteristics of Soil–Rock Mixture in Uniaxial Compression. *Appl. Sci.* **2024**, *14*, 10485. https://doi.org/10.3390/app142210485

Academic Editor: Tiago Miranda

Received: 15 October 2024
Revised: 8 November 2024
Accepted: 12 November 2024
Published: 14 November 2024

1. Introduction

As a special geo-material widely distributed in Southwest China, soil–rock mixture exhibits complex structural characteristics and strength response. Its composition of rock blocks with varying sizes and a soil matrix leads to an extremely heterogeneous loose geotechnical medium system [1,2]. The difference in the mechanical properties between the components means that the rock content becomes a crucial parameter in influencing the mechanical properties of soil–rock mixture by controlling its structure [3,4]. When the rock content is low, the rock blocks remain in a suspended state in the soil matrix and the influence of the varying rock content on strength response and failure mechanism is not obvious. The mechanical properties of soil–rock mixture with a suspended structure are

similar to those of the soil matrix. Conversely, when the rock content is high, a rock skeleton structure is formed and the pores between rock blocks become evident. The contact friction and occlusion between the rock blocks provides the strength for the soil–rock mixture. Previous studies have demonstrated that according to the evolution law of the structural and mechanical characteristics of soil–rock mixture caused by the varying rock content, 25% and 70% were identified as rock content thresholds [5–7]. Unlike homogeneous soil and jointed rock, soil–rock mixture with 25%~70% rock content can be considered a cooperative system of 'soil–rock interface' [3,8]. The appearance of the soil–rock interface due to the varying rock content increases the difficulty of using experimental methods to analyze the evolution law of mechanical characteristics of soil–rock mixture. On the one hand, the influence of the soil–rock interface on the whole material is related to the mechanical properties of the soil matrix and the rock blocks; on the other hand, the quality of the soil–rock interface relevant to the rock content determines the proportion and distribution of weak-strength vulnerable interfaces. Thus, both the influence of the rock content and the soil–rock interface on the strength response and failure mechanism of soil–rock mixture should be analyzed comprehensively from the macro and meso perspectives.

Currently, studies on the influence factors of mechanical characteristics of soil–rock mixture are conducted using in situ tests, laboratory tests, and numerical simulations [9–13]. The mechanical parameters of soil–rock mixture under different loading conditions, such as shear strength, compressive strength, elastic modulus, and so on, have been analyzed. However, the experimental apparatuses (large triaxial compression apparatus or direct shear apparatus) have limitations in observing the failure mechanism of the soil–rock mixture specimen. To observe the process more intuitively, the uniaxial compression test has been commonly utilized to obtain both the failure mechanisms and strength response of soil–rock mixture. Wang et al. [14] and Guo et al. [15] utilized a uniaxial compression test with the help of Computer Tomography (CT) scanning to investigate the evolutionary process of the structural characteristics of soil–rock mixture at the mesoscopic scale. The results indicate that the elastic incompatibility between the soil matrix and rock blocks results in differential sliding on both sides of the interface, which is the fundamental cause of specimen failure. Hu et al. [16] compared the uniaxial compression curves and failure patterns of pure ice, ice–rock mixtures, frozen soil, and frozen soil–rock mixture specimens, concluding that the presence of rock blocks altered the failure pattern from a penetrating tensile crack to a diagonal crack and induced lateral expansion deformation.

Compared to the pure soil specimen, the rock blocks inside the soil matrix can provides resistance to deformation and failure for the whole material. However, the test results above suggest that the occurrence of the rock block destroys the original structure of the soil matrix, leading to the non-homogeneous and discontinuous structural characteristics of soil–rock mixture, especially under uniaxial compression conditions. Afifipour et al. [17] demonstrated that the uniaxial compressive strength (UCS) of soil–rock mixture significantly decreased as rock content increased, with more pronounced ductileness characteristics. Similar findings were also found by Lindquist [18] and Altinsoy [19]. However, the keynote of experimental studies mainly focuses on the effect of varying rock content on the UCS of soil–rock mixture from a quantitative perspective. The mechanism of the derived soil–rock interface on the failure characteristics and strength response of soil–rock mixture is still not sufficiently and comprehensively understood. Given the limitations of experimental methods in discussing the influence of the soil–rock interface, numerical methods have been widely adopted to effectively investigate the destruction process of soil–rock mixture. So far, researchers have chosen continuous medium mechanical calculation methods—such as the finite element method (FEM) [20–22], finite difference method (FDM) [23–25], and numerical manifold method (NMM) [26–28]—as well as discontinuous medium mechanical calculation methods, such as the discrete element method (DEM) [29–31], to analyze the mechanical characteristics of soil–rock mixture under different loading conditions. Based on experimental and simulation results, the neural network method has been widely applied to assess the structural and mechanical characteristics of geotechnical materials, greatly

improving the effectiveness and efficiency of calculations [32–34]. However, compared to the extensive parameter data available for soils or jointed rock, the limitations of soil–rock mixture databases results in prediction outcomes that are not yet comprehensive. Among these, DEM provides an effective approach to simulating the macroscopic mechanical properties of the internal soil, block, and soil–rock interfaces, respectively, by precisely controlling the microscopic contact models among the ball (or block) elements. Additionally, DEM can effectively simulate the large deformation and localized failure processes of S-RM by modeling the breakage and re-connection of contacts between elements, thereby addressing the limitations of the continuous medium mechanical calculation methods and experimental approaches [35,36]. The key to ensuring high accuracy in DEM numerical simulation results lies in developing a precise meso-structure model which can characterize the basic features of the multi-phase compositions of the material. The modeling methods of meso-structure for soil–rock mixture can be broadly classified into the image analysis method and stochastic generation method, depending on how internal rock blocks are generated. The image analysis method constructs the soil–rock mixture model based on processed images, offering higher accuracy. However, this method is time-consuming, costly, and challenging when it comes to acquiring morphological data on rock blocks with a small size. The stochastic generation method, on the other hand, allows for the batch generation of polygonal rock blocks of random sizes based on mathematical statistics and random placement theory. This method requires conflict judgment to prevent rock block overlap, resulting in rock block models that differ from actual distributions [20]. Therefore, the method for generating small, irregular rock blocks based on real block morphology remains a critical challenge in constructing accurate microscopic structural models of soil–rock mixture.

The results of the aforementioned studies indicate that significant progress has been made in understanding the mechanical characteristics of soil–rock mixture under uniaxial conditions. However, the modeling method of the soil–rock mixture meso-structure model considering the influence of the irregular rock blocks remains insufficiently precise, and the mechanism by which rock content and soil–rock interface strength influence UCS are not yet fully understood. To address these gaps, this study aimed to analyze the mechanical characteristics of soil–rock mixture specimens under varying rock contents and soil–rock interface strength using both experimental methods and numerical simulations. First, several uniaxial compression tests were conducted on soil–rock mixture specimens with different rock contents. The influence of rock content on the strength response and failure characteristics of specimens was discussed at the macro scale. Then, to further analyze the meso- mechanism of the internal composition inside the specimen, numerical simulations of uniaxial compression tests on soil–rock mixture were carried out using the particle discrete element method (PDEM). An innovative approach to generating irregular rock block models randomly based on real rock block images was proposed, ensuring that the effect of internal irregular particles is fully considered during the model establishing. The failure characteristics of the soil–rock mixture specimens with varying rock contents and soil–rock interface strengths were identified. Finally, the mechanisms by which strength-influencing factors affect UCS values were discussed from both macro and micro perspectives.

2. Laboratory Uniaxial Compression Test

2.1. Material Properties and Specimen Preparations

The soil–rock mixture used in the test was collected from the Taoyuan-Jinshajiang bridge site, located in Yunnan Province, China (Figure 1). Two representative sampling locations, along with their basic physical properties, are listed in Table 1. Geotechnical data indicate that the engineering geological strata of the deposit slope near the bridge site are relatively complex, and the uppermost stratum is composed of Quaternary avalanche deposit, predominantly consisting of soil–rock mixture. The soil is silty clay with a brown-red to brown-yellow color, exhibiting a hard plastic consistency. The rock blocks consist

of moderately weathered limestone, primarily angular to sub-angular in shape, with a variable particle size distribution.

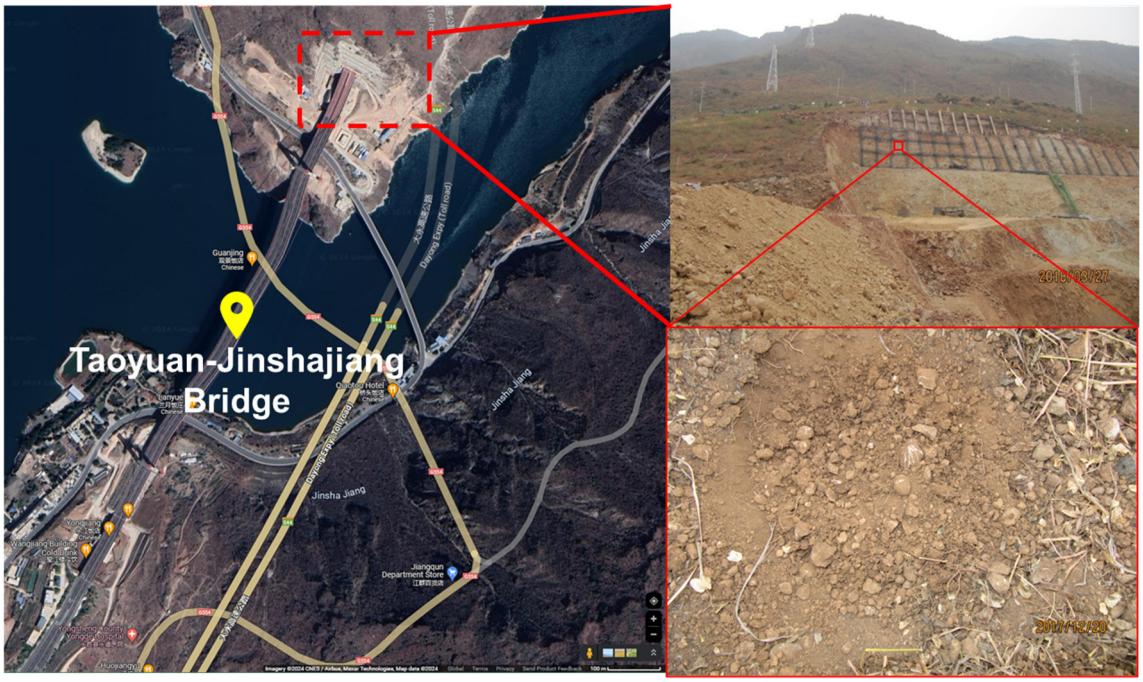

Figure 1. Location and geological conditions of the study area.

Table 1. The properties of the experimental materials.

Sampling Location	In Situ Density, ρ/(kg/m^3)	Natural Water Content, ω/(%)	Dry Density, ρ_s/(kg/m^3)	Permeability Coefficient, k_s (m/s)
East side of the slope	1555	2.39	1519	3.67×10^{-3}
Northeast corner of anchor pit	1622	2.21	1585	2.84×10^{-3}

Particle grading tests for soil–rock mixture from two sampling locations were conducted as shown in Figure 2a. The results indicate that the maximum size of the geomaterial in the study area is 60 mm, with coefficient of curvature (Cc) and uniformity coefficient (Cu) values listed in Table 2. These values suggest that the particle grading of the soil–rock mixture in the study area is discontinuous and exhibits a poorly graded condition. The particle size distribution histograms are presented in Figure 2b, revealing a bimodal characteristic in the particle size distribution. A significant decrease in mass content is observed in the particle size range of 1~2 mm. According to the soil–rock threshold determination method proposed by Medley [37], the threshold of soil and rock, dS-RT, should be set at 0.05 Lc, where Lc represents the characteristic length of the study area. This threshold determination method indicates that dS-RT is not constant; for in situ uniaxial compression specimens, the diameter of the test specimen can be chosen as Lc, which in this study is 6.18 mm. As for the specimen for the uniaxial compression test in this study, 3.09 mm should be chosen as soil/rock threshold. Considering the size limitations of screening equipment and the specifications of the soil test (SL237—1999) [38], the dS-RT of soil–rock mixture specimen in this study was selected as 2 mm, and the maximum diameter of the rock blocks should be less than 10 mm (Figure 3).

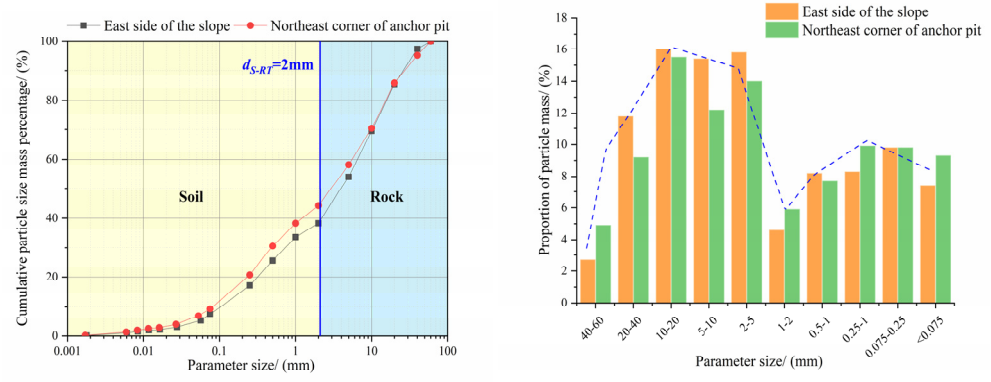

(**a**) (**b**)

Figure 2. (**a**) Grading curves and (**b**) particle size distribution histograms of soil–rock mixture from different sampling locations.

Table 2. Grading indexes of soil–rock mixture from different sampling locations.

Sampling Location	Coefficient of Curvature, *Cc*	Uniformity Coefficient, *Cu*
East side of the slope	0.48	56.82
Northeast corner of anchor pit	0.71	67.27

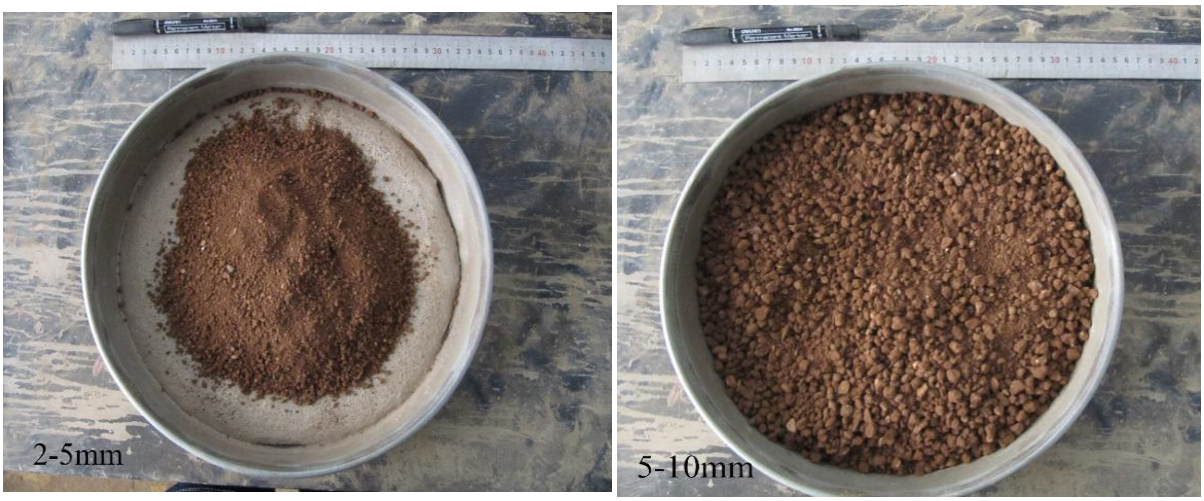

(**a**) (**b**)

Figure 3. Rock blocks for uniaxial compression test with size of (**a**) 2–5 mm and (**b**) 5–10 mm.

2.2. Test Apparatus and Scheme

The uniaxial compression test of soil–rock mixture was conducted using a servo-controlled soil triaxial apparatus with a maximum loading force of 2 kN. Axial loading was applied to the specimen using displacement control at a rate of 1.1 mm/min. The particle grading curves indicate that the rock content of the soil–rock mixture in the study area ranged between 50% and 60%, suggesting that the rock content of the specimens prepared for the uniaxial compression test should also be set between 0~60%. However, during the sampling process, it was found that weak cohesion between the soil matrix and rock blocks made it challenging to mold soil–rock mixture specimens with high rock content. Consequently, the maximum rock content selected for this test was 30%.

Before specimen preparation, the volume of soil matrix and rock blocks was determined according to the test scheme as listed in Table 3. The volumetric rock content was

selected as the rock content control index. In the specimen preparation process, the reference specimen with 0% rock content (pure soil specimen) was first prepared to obtain the density of the soil. By replacing the soil in the 0% rock content specimen with an equivalent volume of "rock", soil–rock mixture specimens with varying rock contents were prepared. To better illustrate the particle distribution characteristics of the experimental material, the constrained grain size (D_{60}) and effective grain size (D_{10}) were determined based on the provided particle distribution curves. The constrained grain size, D_{60}, refers to the particle size below which 60% of the total mass of the material is comprised. Similarly, the effective grain size, D_{10}, represents the particle size below which 10% of the total mass of the material is comprised [39,40].

Table 3. Test scheme of soil–rock mixture with varying rock contents.

Test Number	Rock Content/(%)	Volume of Rock Blocks/(cm^3)	Volume of Soil/(cm^3)	Mass of Water/g	D_{60}/ mm	D_{10}/ mm
1	0	0.0	375.0	61.3	0.232	0.014
2	5	18.8	356.3	54.8	0.25	0.014
3	10	37.5	337.5	49.1	0.32	0.016
4	15	56.3	318.8	45.2	0.39	0.016
5	20	75.0	300.0	50.9	0.48	0.016
6	25	93.8	281.3	43.3	0.65	0.018
7	30	112.5	262.5	38.8	0.87	0.020

The maximum dry density and optimum water content were utilized to ensure optimal mechanical properties, as well as comparability and high reproducibility. In various construction projects, such as subgrade slopes or dam construction, compacted soils typically approach the state defined by their optimum moisture content and maximum dry density. Therefore, the specimens in this study were prepared under these conditions, resulting in relatively higher strength. Compaction tests for soil–rock mixtures with varying rock contents were conducted using a heavy compaction apparatus, yielding the maximum dry density and optimal moisture content for each rock content condition. The optimal moisture content was then used as the target moisture content to determine the required water mass for the specimen preparation as shown in Table 3.

The soil and rock blocks were initially placed in a drying oven for drying. Following this, the calculated amount of water was sprayed onto the soil matrix and rock blocks. After thorough mixing, the required soil–rock mixture was placed in a closed container for at least 24 h to ensure uniform water content. The geo-material mass was determined based on the dry density and placed into a mold measuring 125 mm × 61.8 mm in five layers. Compaction was performed until each layer reached the required height, and the surface was shaved before adding the second layer. This process continued until the final layer was compacted, resulting in the soil–rock mixture specimen shown as Figure 4.

2.3. Test Results

2.3.1. Influence of Rock Content on Failure Characteristics Under the Compression Testing

The uniaxial compression axial stress–strain curves for the seven groups of soil–rock mixture specimens with varying rock contents are shown in Figure 5. The results indicate that the curves exhibit a similar trend under varying rock content conditions, which can be divided into five distinct stages. In the initial stage of axial loading (OA stage), the axial stress shows a slightly upward concave trend at a small scale. The specimen then rapidly presents the linear elastic characteristics in AB stage until a stress drop occurs after reaching the peak compressive strength (as BC stage shown). During the CD and DE stages, the axial stress gradually decreases at a slower rate. The soil–rock mixture specimens exhibit various failure characteristics at different stages. In the OA and AB stages, no significant cracks were observed on the specimen surface, but localized fracture appeared once peak strength

was reached (Figure 5). As the axial strain increased, cracks on the surface expanded rapidly until the main cracks penetrated (Figure 5).

Figure 4. Sample preparation and test equipment.

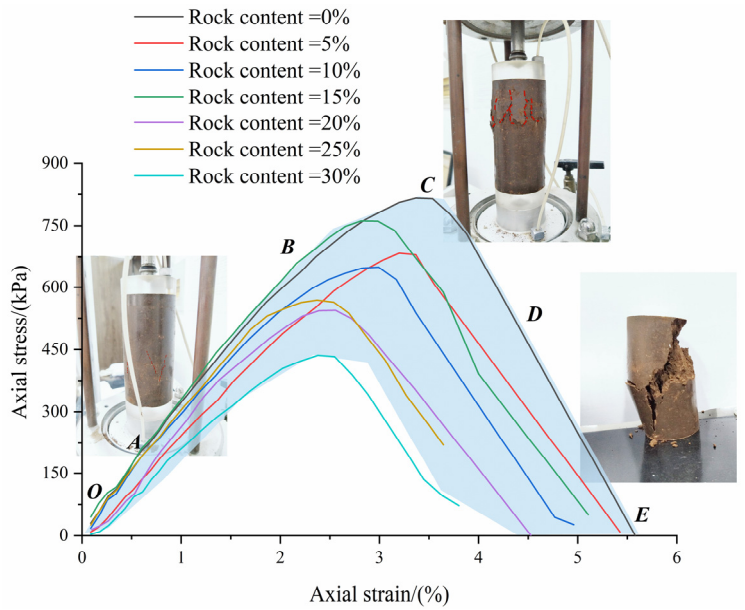

Figure 5. Axial stress–strain curves and crack distributions of soil–rock mixtures with varying rock contents (the red dashed lines indicate the visible crack).

The specimens with varying rock contents exhibited varying failure modes, as illustrated in Figure 6. These failure modes can be categorized into three types: longitudinal fracture, shear fracture, and multiple shear fracture. The soil–rock mixture specimens with 0~15% rock content displayed a main crack that penetrated through the specimen (Figure 6a). As the rock content increased, the distribution of rock blocks within the specimens became more pronounced, resulting in a greater number of cracks that tended to become disorganized upon failure (Figure 6b). Under a rock content of 30%, the cracks on

the surface primarily expanded around the rock blocks, leading to a multiple shear fracture without a prominent through crack, as shown in Figure 6c.

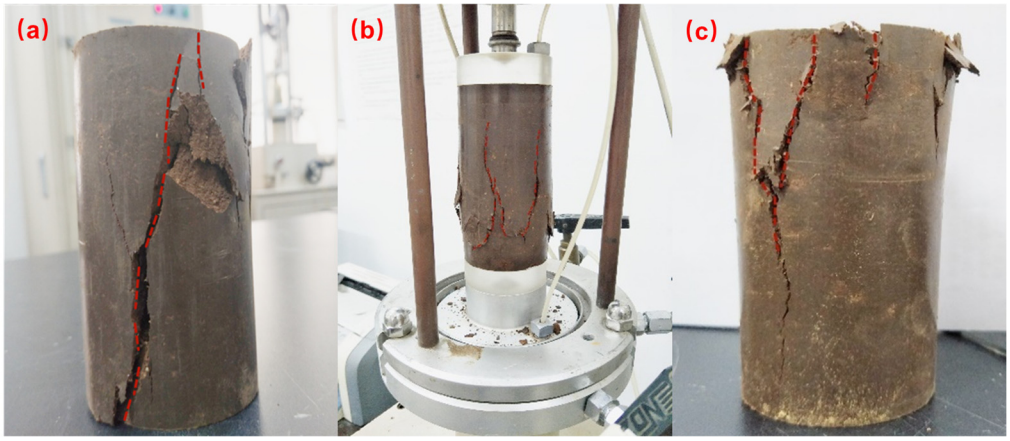

Figure 6. Failure modes of soil–rock mixture specimens with varying rock contents as (**a**) longitudinal fracture; (**b**) shear fracture; (**c**) multiple shear fracture.

2.3.2. Influence of Rock Content on Strength Responses Under Compression Testing

Table 4 presents the elastic modulus, UCS, and the axial strain corresponding to the UCS of the soil–rock mixture specimens with varying rock contents. The incorporation of rock blocks within soil–rock mixture significantly enhances its resistance to deformation induced by external forces compared to the pure soil material. However, the mechanical properties of soil–rock mixture exhibit a notable deterioration trend as rock content increases, particularly when the rock content exceeds 15%. Figure 7 illustrates that the elastic modulus, UCS, and the axial strain corresponding to UCS exhibit a distinct decreasing trend as the rock content increases. Notably, the latter two indices present exponential and linear decline, respectively. Additionally, the time required for the specimen to achieve uniaxial compression strength (UCS) and complete failure consistently decreases as rock content increases.

Table 4. Mechanical properties of soil–rock mixture with varying rock contents.

Index	**Value**						
Rock content/(%)	0	5	10	15	20	25	30
Elastic modulus/MPa	24.29	21.45	21.73	24.92	21.28	24.00	18.32
UCS/kPa	816.24	684.14	650.09	701.46	544.17	568.79	435.75
Axial strain corresponding to UCS/(%)	3.36	3.19	2.99	2.82	2.56	2.37	2.38

From the point of view of material composition, the appearance of a rock block should provide strength for the whole material through its own strength on one hand and through cooperation with the soil matrix and other rock blocks on the other hand. However, under uniaxial compression conditions, the soil–rock interface derived from the emergence of the rock block plays a negative role in the mechanical characteristics. The failure mode of the soil–rock mixture specimen with 30% rock content indicates that local failures predominantly occur near the rock blocks, with cracks propagating along the soil–rock interface, resulting in complex crack distributions. The strength of soil–rock mixture under the uniaxial compression conditions compared to that of the soil matrix also decreases, which means the strength provided by the increasing soil–rock interface is obviously weaker than that of the initial soil matrix. Additionally, the decrease in mechanical properties becomes more pronounced as rock content exceeds 15%, which correlates with the particle distribution characteristics. As shown in Table 3, the D_{60} value increased rapidly from about 0.3 mm to 0.87 mm as the rock content rose from 10% to 30%. Previous researches

have indicated that particle sizes ranging from D_{10} to D_{60} play a critical role in the forming of the soil skeleton. With increasing rock content, the particle size that governs the structure of the soil–rock mixture also increases, and for materials with high rock content, rock blocks play a vital role in defining structural characteristics. The disturbance influence of rock blocks and the soil–rock interfaces on the soil matrix becomes more evident.

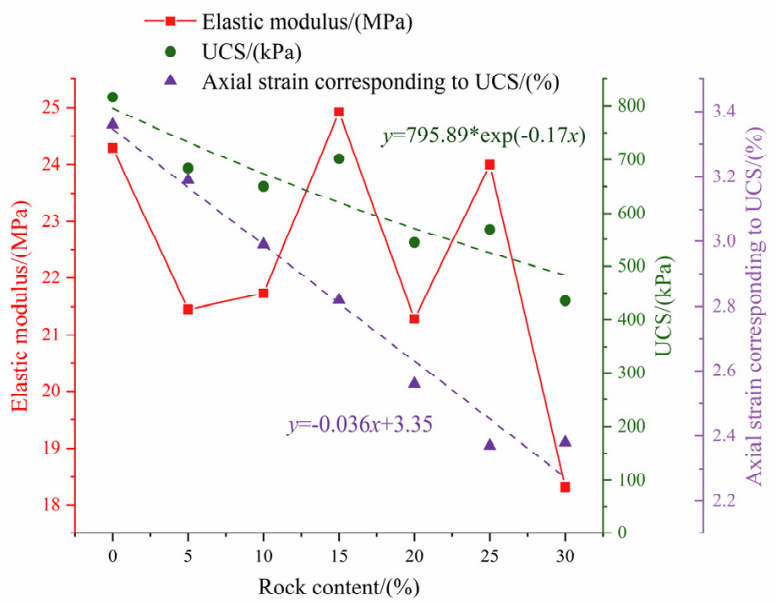

Figure 7. Mechanical characteristics of soil–rock mixture with varying rock contents.

Therefore, the soil–rock interface presents complex and variable influence on the mechanical characteristics of soil–rock mixture, and its mechanism represent critical issues warranting further analysis.

3. Meso Analysis of Mechanical Characteristics of Soil–Rock Mixture

The experimental results above indicate that the soil–rock interface is closely associated with the mechanical characteristics of soil–rock mixture. As a theoretical concept, the soil–rock interface is intricately linked to the cohesion of the soil, the roughness of the rock block surfaces, and the degree of the bonding between soil particles and rock blocks. To effectively characterize the heterogeneous and discontinuous meso-structure characteristics, this study utilized PDEM to simulate the macro mechanical properties of soil–rock mixture through particle contact modeling at the meso-scale.

In PDEM, regular disks (in 2D) and balls (in 3D) are selected as the fundamental elements, with the contact models between particles and their parameters established based on experimental results. By applying Newton's laws of motion, the displacement and contact forces of the particles can be calculated.

3.1. Meso-Structure Model Generation of Soil–Rock Mixture

3.1.1. Generation of Irregular Rock Block Model

Geological survey results indicate that the rock blocks within the deposit slope are angular and exhibit uneven surfaces. Previous irregular rock block model generation methods have primarily relied on the mathematical and statistical results of the shape indices derived from the rock block morphology. While these methods facilitate the batch generation of rock blocks of varying sizes, they require a substantial amount of shape indices. However, it is important to note that collecting and processing image data for small-sized irregular rock blocks, as shown in Figure 3, presents considerable challenges, often resulting in shape indices with low accuracy. To address the particle size issue, this study employs shape fractal theory. It is posited that, as a natural geological product,

the particle size distribution and surface distribution of soil–rock mixture exhibit distinct fractal characteristics, demonstrating self-similarity. Accordingly, rock blocks sized between 2~10 mm and 20~50 mm share the similar geometric morphologies based on the fractal theory, allowing the shape indices of the former to be determined by scaling the particle size of the latter. The rock blocks with a long axis ranging from 20 to 50 mm, collected from the deposit slope near the Taoyuan-Jinshajiang bridge site, were used as the generation template, as illustrated in Figure 8a.

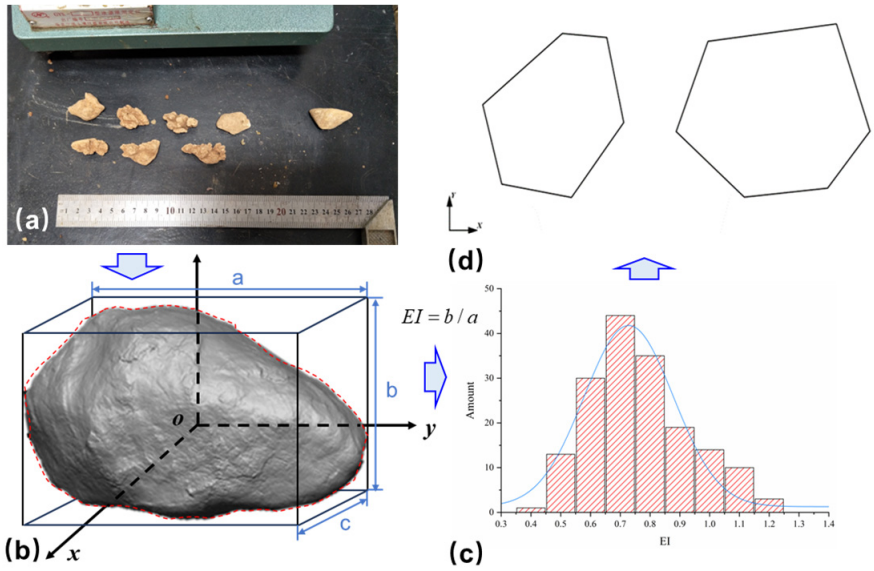

Figure 8. (**a**) Real rock blocks; (**b**) three-dimensional reconstruction; (**c**) distribution of EI of rock blocks; (**d**) base plane of irregular rock block models.

To accurately capture the geometric characteristics of the irregular blocks, a 3D handheld laser scanner (RS100S) was used to perform three-dimensional imaging and scanning of the rock blocks. The measurement accuracy of the 3D handheld laser scanner is between 0.005 mm and 0.015 mm, allowing for precise capture of the spatial point cloud on the outer surface of the rock blocks. The point cloud processing module and simplification function were then applied to obtain the accurate geometric shapes of the rock blocks with varying particle sizes. The three sides of the external cuboid of the irregular rock blocks correspond to the major axis, the central axis, and the minor axis, respectively, with the shape indices of the irregular rock blocks related to these three principal axes. The ratio of the central axis to the major axis is defined as the Elongation Index (*EI*), while the ratio of the minor axis to the central axis is referred as the Flatness Index (*FI*), as shown in Figure 8b. The calculation equations of *EI* and *FI* are expressed as follows:

$$EI = b/a \tag{1}$$

$$FI = c/b \tag{2}$$

where a represents the major axis, b the central axis, and c the minor axis. The values of *EI* and *FI* range from 0 to 1. The closer the value is to 0, the flatter the shape of the rock block. Conversely, the closer the value is to 1, the more the rock block resembles a sphere.

The base surfaces of the selected rock blocks are mainly convex polygons in order to improve calculation and modeling efficiency. The *EI* and *FI* values of rock blocks within the 20~50 mm size range were determined using digital image analysis. Given that the focus of the simulations in this paper is the mechanical characteristics of soil–rock mixture under two-dimensional plane conditions, the *EI* index was selected as the key parameter to represent the shape of the rock blocks. The probability distribution of the *EI* shape index is

illustrated in Figure 8c, showing that *EI* values range from 0.65 to 0.8, with a concentration around 0.7. Based on these statistical results, two typical rock blocks with *EI* values of 0.75 and 0.85 were selected as templates (Figure 8d) for establishing irregular rock block models in 2D to explore the mechanical characteristics of soil–rock mixture under uniaxial compression conditions.

3.1.2. Generation of Soil-Rock Mixture Model

Before generating the meso-structure model of soil–rock mixture with irregular rock blocks, it is essential to determine the threshold of the soil and rock blocks. Given that the number of particles in the model significantly affects calculation efficiency, 2 mm was selected as the soil/rock threshold in the numerical simulations in this study. Regular disk elements were chosen to simulate the soil matrix, with a diameter range of 1~2 mm. Irregular rock block particles ranging from 2~10 mm were randomly placed using the generation method proposed above, consistent with the actual test conditions.

The results of the laboratory uniaxial compression tests indicate that the rock blocks exhibit no discernible fragmentation throughout the test process. Consequently, the irregular rock block models in the PDEM simulations are constructed using clump elements, which are commonly used to create irregular geometries by overlapping combinations of regular circular particles. The particle diameter ratio and overlap distance of the filled particle can be adjusted to enhance the shape similarity between the rock block model and the actual rock. It is important to note that the equivalent diameter size of the clump element matches the equivalent diameter of a disk element with the same volume. The detailed steps for generating the soil–rock mixture meso-structure model with irregular rock blocks are as follows:

(a) The pure soil meso-structure model is constructed with a height of 12.5 cm and a width of 6.18 cm, as shown in Figure 9a. The disk elements were utilized to simulate the pure soil as shown by the blue disk in Figure 9a. The wall elements are defined as rigid, with the normal stiffness and friction coefficient set to 0 to minimize friction effects caused by the boundaries.

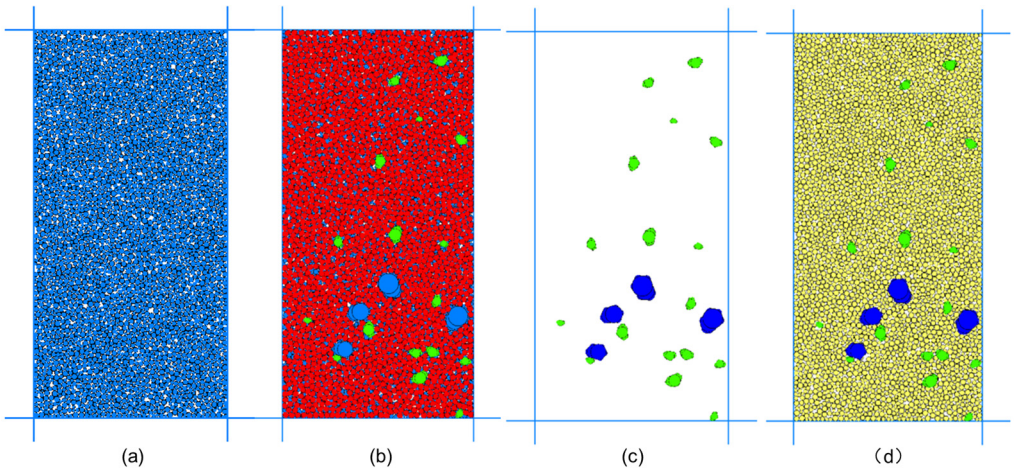

Figure 9. Meso-structure models of (**a**) pure soil; (**b**) soil mixed with overlapping rock blocks; (**c**) rock blocks; (**d**) soil–rock mixture without any overlap.

(b) Ensure that all soil particles reach equilibrium before putting the regular (the red disk element) and irregular rock block (the green and blue clump element) particles in groups. During the placement process, it is crucial to ensure that the rock block particles do not extend beyond the model boundaries or overlap with existing rock block particles. The volume proportion of irregular rock blocks, referred to as the rock content, is used as the control index for the placement of rock blocks. Once the target

rock content is achieved, several balancing iterations are initiated until the rock blocks within the specimen reach equilibrium (Figure 9b).

(c) Identify and remove the regular rock blocks that overlap with the irregular rock blocks and all the soil particles, utilizing the group and disk element pointer research command, as illustrated in Figure 9c.

(d) The remaining particles, including the soil particles (yellow disk elements) and the irregular rock blocks (the green and blue clump elements),within the specimen are then re-cycled to achieve equilibrium, ensuring that the ratio of the average unbalanced force to the total contact force is less than 10–6 through the application of the wall servo command. Ultimately, the soil–rock mixture meso-structure model is generated, incorporating the irregular rock block models based on the actual shape of the rock blocks, as depicted in Figure 9d.

3.2. Calibration of the Meso-Parameter

To characterize the differences in mechanical properties between real soil and rock particles, as well as the structural heterogeneity of soil–rock mixture, contact bond strength models with varying meso-parameters were calibrated. The parameter calibration was primarily conducted using the trial–error method to ensure the simulation results closely aligned with the experimental results, ultimately obtaining a group of representative meso-parameters. First, the meso-parameters of the bond contact model between soil–soil particles were calibrated based on the experimental results of the pure soil specimen (with a rock content of 0). Next, the meso-parameters of the rock–rock and soil–rock contact models were calibrated using the experimental results of the soil–rock mixture with 30% rock content. Consequently, all meso-parameters of different types of particle–particles and particle–wall were obtained, as listed in Table 5.

Table 5. Meso-parameters of the soil mixture numerical model.

Contact Type	Contact Name	Contact Normal Stiffness, k_n/(N·m^{-1})	Normal-to-Shear Stiffness Ratio, k_n/k_s	Shear Strength, $F_n{}^c$	Tensile Strength, $F_s{}^c$	Friction Coefficient, μ
Particle–particle	Soil–soil	3.0×10^7	1	1100	900	0.3
	Rock–rock	3.5×10^7	1	500	500	0.9
	Soil–rock	3.0×10^7	0.5	1000	800	0.7
Particle–wall	Soil–wall	1×10^7	0.0	—	—	—
	Rock–wall	6.5×10^7	0.0	—	—	—

During the simulation process, the walls on both sides of the model were first removed, transitioning the simulation condition to uniaxial compression. The axial loading speed of the wall was then set to 0.005 m/s, and the uniaxial compression simulation test of soil–rock mixture was performed. The test was terminated when the post-peak axial stress dropped to 0.7 times the peak strength. The simulation results of soil–rock mixture with varying rock contents are presented in Figure 10. The results demonstrate that, for the same rock content and specimen size, the axial stress–strain curves obtained from the simulations closely resemble experimental results, exhibiting a clear linear increase followed by strain-softening behavior. Despite some discrepancies between the simulation and experimental results (such as the strain corresponding to the peak strength), the relative error values of the UCS are within 10%. This suggests that the meso-structure model of soil–rock mixture with irregular rock blocks generated in this study can more accurately reflect the real structure and mechanical characteristics of the soil–rock mixture.

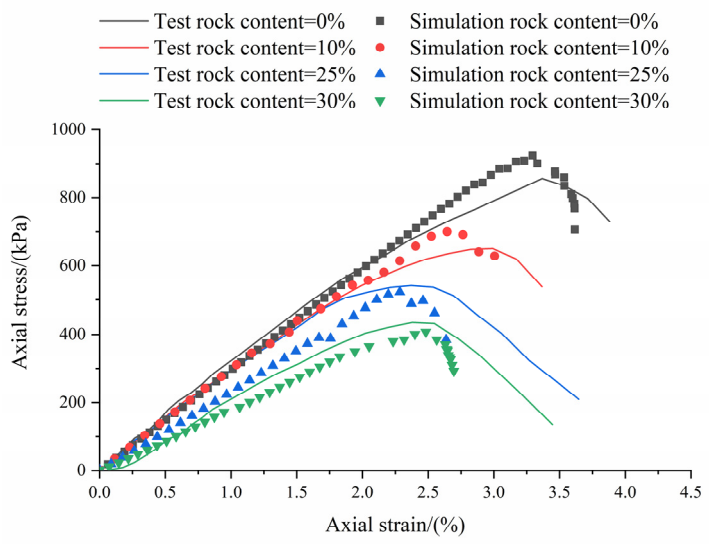

Figure 10. Axial stress–strain curves of the simulation and experimental results.

4. Failure Mechanism of Soil–Rock Mixture at the Meso-Scale

4.1. Failure Mechanism of Soil–Rock Mixture with Varying Rock Contents

The state at which the post-peak strength drops to 0.7 times the peak strength is defined as the failure state. In the pure soil model, the displacement direction deviation of particles is evident on both sides of the red dotted line shown in Figure 11a. Particles in the lower-middle region are observed to separate from the model, while the left region is dominated by lateral expansion, with particle displacement occurring primarily in the horizontal direction. The failure characteristics changes when a certain amount of high-strength rock blocks are present in the soil matrix. In the model with a low rock content (5%), significant contact failure and particle movement are observed in the lower region of the model in contact with the wall. The model can be divided into three zones: zones ①, ②, and ③ (Figure 11b). The displacement vectors of the rock blocks distributed on both sides of the long crack (the dividing line between zones ② and ③) differ significantly from those of the nearby soil particles. The displacement vector diagram shows that rock blocks gradually control the particle displacement direction and the location of local failure. Soil–rock contacts are more prone to fracture, leading to particle separations. The local failure of soil–rock mixture primarily initiates at the soil–rock contact surfaces, with slightly lower strength under uniaxial compressions.

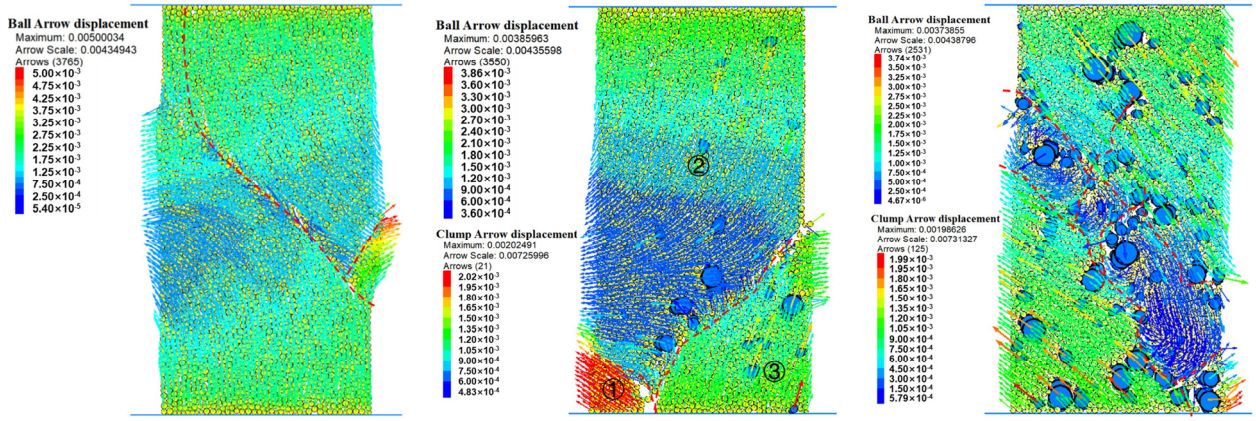

(**a**) (**b**) (**c**)

Figure 11. Displacement vector diagram of soil–rock mixtures with rock content of (**a**) 0%, (**b**) 5%, and (**c**) 30% at the failure state.

Figure 11c shows that the distribution of displacement direction in the soil–rock mixture model with rock content of 30% is more disordered. As the rock content increases, the likelihood of rock blocks being distributed both inside and on the surface also increases, significantly influencing the failure mechanism of soil–rock mixture. In addition to the two main cracks extending from the upper left to the lower right, vertical tensile cracks are present, and the shape of the cracks is more irregular. Due to the weaker strength at soil–rock contacts, bonding failure tends to occur first at these interfaces. During crack propagation, phenomena such as branching, intersection, and interlocking arise due to obstruction by surrounding rock blocks. The cracks then continue to propagate into the weaker soil matrix, ultimately leading to the formation of multiple shear fractures. Some of the rock blocks and surrounding soil particles become embedded and bound together, forming local soil–rock clusters. These clusters moved as a unit under axial stress, with damage occurring either at the weaker soil–rock interface or within the soil matrix, leading to lateral expansion and local detachment.

In summary, as rock content increases, the soil–rock interfaces generated within the soil–rock mixture bear external forces alongside the soil matrix and rock blocks, forming an internal "soil–rock block interface" system. The relatively weak strength of these soil–rock interfaces makes them the primary path for local failure and crack propagation under uniaxial compression. As a result, the failure pattern gradually shifts to being controlled by the rock blocks, ultimately leading to a transition in the failure mode of the soil–rock mixture from longitudinal fracture to multiple shear fractures.

4.2. Failure Mechanism of Soil–Rock Mixture with Varying Soil–Rock Interface Strength

The simulation results indicate that the formation of soil–rock interfaces is a key factor contributing to the high complexity of the failure characteristics of soil–rock mixture as rock content increases. As a unique virtual parameter of soil–rock mixture, the strength of the soil–rock interface is closely related to the mechanical properties of both the soil matrix and the rock blocks, making it difficult to control and characterize intuitively during testing. Therefore, to further analyze the influence of soil–rock interface strength on the failure mechanism, uniaxial compression simulation tests were conducted with varying contact strengths by adjusting the friction coefficient of the soil–rock contact model.

Figure 12 shows the force chain distribution contours of soil–rock mixture models at the failure state with varying friction coefficients of soil–rock contacts. The results reveal that when the friction coefficient of soil–rock interfaces is high, the soil matrix, rock blocks, and interface collectively enhance the ability of the material to resist external deformation. The thickness of the internal force chains is relatively uniform and predominantly concentrated in the soil–rock contact areas. As the friction coefficient decreases, the strength provided by the soil–rock interface also diminishes, resulting in the force chain becoming predominantly concentrated in the middle and lower parts of the left side of the model. In comparison to the strong chain observed at the soil–rock interface in Figure 12a, the strong chains depicted in Figure 12c,d are predominantly located within the soil matrix. Furthermore, the uneven distribution of internal force chains within the soil–rock mixture becomes increasingly pronounced, resulting in a heightened probability of contact fractures at the weaker soil–rock interface.

The force chain distributions of soil–rock mixture models with varying soil–rock interface strength suggest that under conditions of low friction coefficients, the soil matrix remains the primary contributor to the strength of soil–rock mixture. From a mesoscopic perspective, the reduction in strength at the soil–rock interface significantly diminishes its capacity to transfer bearing loads effectively. The improvement of the soil–rock contact failure probability leads to a macroscopic manifestation characterized by pronounced tensile cracking and rapid failure of the model. As the soil–rock contact strength increases, the soil–rock interface gradually becomes more influential on the strength of the whole soil–rock mixture, and the contact failure probabilities of the soil–soil, soil–rock, and the

rock–rock contacts also become closer. The failure of the model is mainly through crack, and the ability to resist external force deformation is also stronger.

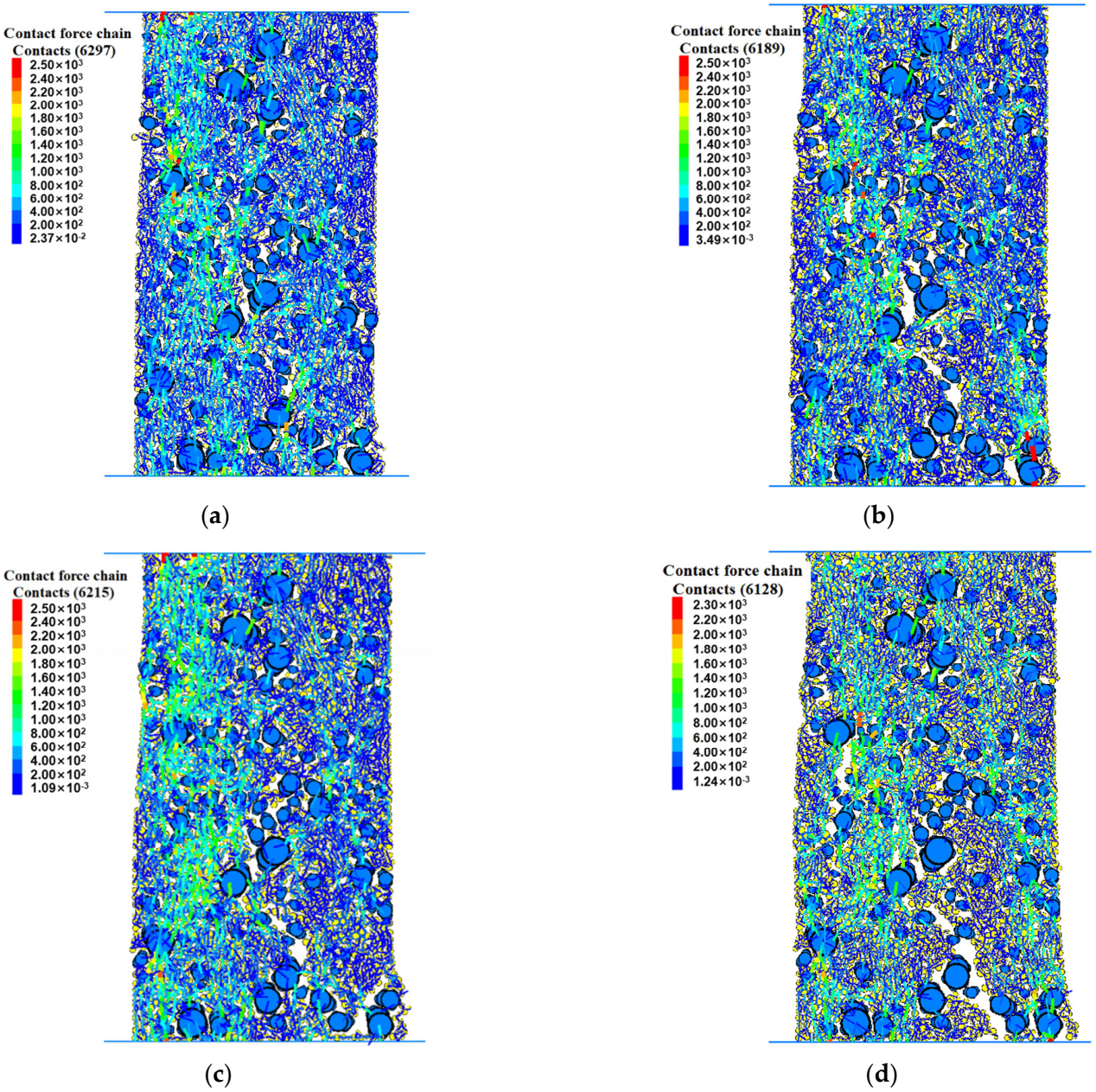

Figure 12. Force chain distributions of soil–rock mixture with a friction coefficient of (**a**) 0.9, (**b**) 0.5, (**c**) 0.3, and (**d**) 0.1 under the uniaxial compression condition.

5. Influencing Factors of Strength Responses of Soil–Rock Mixture

In accordance with the methodology for determining strength in the uniaxial compression test on rock, the peak strength of the axial stress–strain curve of soil–rock mixture is identified as the UCS value. The UCS values for soil–rock mixtures with varying rock contents, derived from computer numerical simulations, are presented in Table 6. The results demonstrate that as rock content increases from 0 to 30%, the UCS exhibits a rapid exponential decline, decreasing from 923.62 kPa to 407.67 kPa. Correspondingly, the axial strain at which UCS occurs also decreases, from 3.29% to 2.03%.

Table 6. UCS values of soil–rock mixtures with varying rock contents based on the computer simulation.

Rock Content/(%)	UCS/(kPa)	Axial Strain Corresponding to UCS/%
0	923.62	3.29
5	853.66	3.11
10	700.02	2.64
15	665.97	2.67
20	634.80	2.64
25	522.59	2.27
30	407.67	2.03

The discussions above show that underlying cause of the decrease in strength of soil–rock mixture triggered by an increase in rock content is the emergence of weak-strength soil–rock contact surfaces. Figure 13 illustrates the variation in UCS of soil–rock mixture models with varying rock contents under various friction coefficients of soil–rock contact. The results indicate that the UCS consistently declines as the friction coefficient decreases under different rock content conditions. Additionally, the sensitivity of UCS to variations in the friction coefficient varies significantly with different rock contents. Under conditions of low rock content (5%), the UCS decreases from 947.56 to 842.43 kPa, representing a reduction of 11.09% as the interface friction coefficient decreases from 0.9 to 0. Conversely, at the rock content of 30%, the UCS decreases from 417.63 kPa to 243.37 kPa, reflecting a substantial reduction of 41.73% as the friction coefficient decreases.

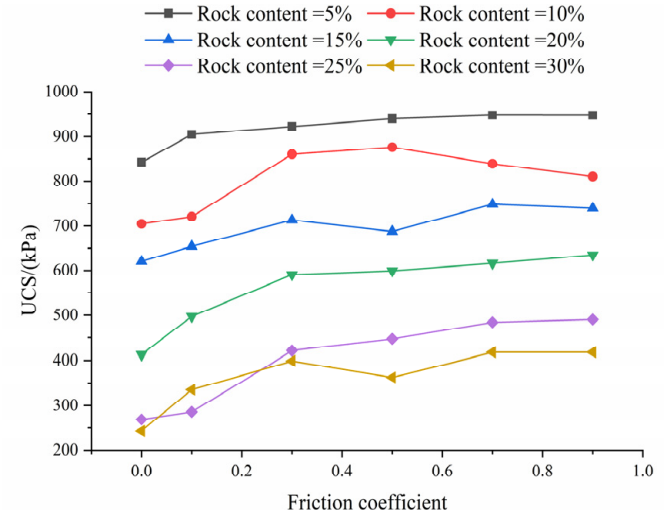

Figure 13. Relationship between UCS and interface friction coefficient of soil–rock mixtures with varying rock contents.

The variation trends of UCS indicate that both rock content and soil–rock interface strength significantly influence UCS. From the perspective of material stiffness, the increase in rock content facilitates a gradual transition in the mechanical properties of soil–rock mixture from those of soil to those of a jointed rock mass, resulting in enhanced material stiffness. To quantitatively assess the influence of rock content and soil–rock interface strength on UCS, this paper discusses the disturbance effect of rock content by considering how rock blocks damage the initial structure of the soil matrix. The strength disturbance ratio ($\sigma_{S\text{-}RM}/\sigma_c$) is defined as the ratio of UCS between the soil–rock mixture and the soil matrix. Figure 14 presents the variation in the strength disturbance ratio of UCS with rock content of soil–rock mixture under varying friction coefficients. An exponential function of the form $y = A \times Bx$ was used to fit the UCS variation, and the resulting estimated formulae for UCS of soil–rock mixture are shown in Figure 14.

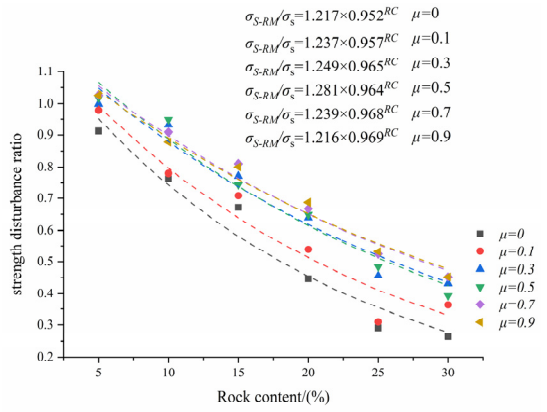

Figure 14. Disturbance ratio of UCS of soil–rock mixture with varying interface friction coefficients and rock contents.

Figure 15 presents the relationship curves between the parameter A and B in the estimation formula and the friction coefficient of the interface. The results reveal clear functional relationships between these undetermined parameters and friction coefficient, as follows:

$$A = -0.249\mu^2 + 0.222\mu + 1.216 \quad (3)$$

$$B = 0.969 - 0.017 \times 0.025^{\mu} \quad (4)$$

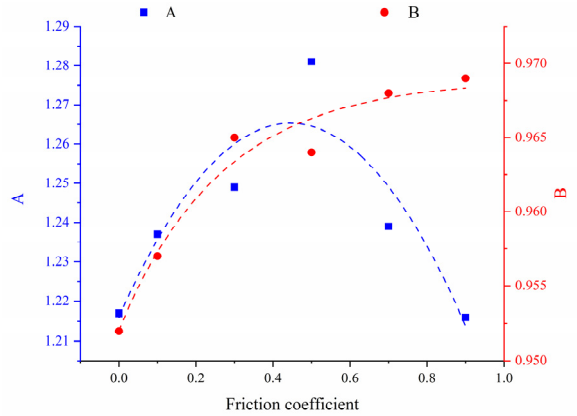

Figure 15. Relationship between parameters A and B and interface friction coefficient.

The results in Figure 15 demonstrate that as the friction coefficient of the interface increases, the parameter A exhibits a parabolic trend, and the values of parameter A are relatively close. Based on Equations (3) and (4) and the variation laws in Figure 14, it can be concluded that the sensitivity of the parameter A to changes in the interface friction coefficient is low, and its variation has a relatively minor impact on the compressive strength disturbance caused by the presence of rock blocks. Parameters A and B can be regarded as undetermined parameters to describe the strength of the soil–rock interface. The strength of the soil–rock interface is closely related to the strength characteristics of the soil matrix, as well as the shape and roughness of the rock blocks. Therefore, it is suggested that the parameter A is primarily associated with the strength characteristics of the soil matrix of soil–rock mixture.

In contrast, the undetermined parameter B is more sensitive to changes of the interface, exhibiting an exponential increase as the friction coefficient rises. Based on the UCS estimation formula, it can be concluded that the increasing rock content significantly reduces the disturbance effect on the soil matrix structure and UCS as parameter B increases. This indicates a close relationship between the undetermined parameter B and the rock blocks. The friction coefficient of the interface, being a microscopic parameter, correlates

with the roughness of the rock block particles at the macroscopic level. Therefore, parameter B can be considered related to the roughness of the rock blocks. When the rock block roughness is high, the resulting soil–rock interface attains a certain strength, and the disturbance of rock content on UCS is relatively low. This finding is consistent with the UCS estimation formula proposed in this paper.

6. Conclusions

This paper investigated the mechanical characteristics of soil–rock mixture under uniaxial compression conditions, from both macro- and meso-mechanical perspectives. The mechanical properties of soil–rock mixtures with varying rock contents and soil–rock interface strength were discussed based on experimental and simulation results, and the mechanisms of the two key influence factors on mechanical characteristics were explored in detail. The findings provide valuable insights for understanding the mechanical properties of soil–rock mixture in the Yunnan region and for mitigating geological hazards on deposit slopes. The main conclusions are as follows:

(1) At the macro-scale, the axial stress–strain curves of soil–rock mixture specimens with varying rock contents exhibited similar behaviors under uniaxial compression conditions. The axial stress presented a distinct stress drop, with specimen failure occurring primarily during the peak strength and stress drop stages, characterized by surface soil detachment and penetration failure. As the rock content increased, the failure characteristics of the soil–rock mixture specimen changed from a dominant crack that penetrated through the material to a more complex multiple shear fractures, as rock blocks gradually played a critical role in the localized destructions.

(2) At the meso-scale, a generation method for irregular rock block models based on the morphology of real rock blocks was proposed. The rock content and the meso-parameters of the contact model between the soil and rock block particles were analyzed to identify the key factors influencing the mechanical characteristics of soil–rock mixture. For the rock content, the distribution of internal force chains became more uneven, with greater concentration in the soil–rock contact areas as the rock content increased. This made these regions more susceptible to contact-induced fractures. For the soil–rock interface strength, the likelihood of contact failure between soil and rock particles significantly increased as the friction coefficient of the interface decreased, making the rock blocks more prone to rolling and displacement within the soil matrix.

(3) Experimental and simulation results show that the UCS value and the associated axial strain of soil–rock mixture decreased exponentially as the rock content increased. Furthermore, as the friction coefficient of the interface decreases, the disturbance effect of rock content on UCS became more pronounced. An estimation formula for UCS of soil–rock mixture, influenced by rock content and the soil–rock interface strength, was developed. Analysis of the interrelationships between the macroscopic roughness of rock block particles, the strength characteristics of the soil matrix, and the microscopic contact surface friction coefficient clarified the physical significance of the parameters used in the estimation formula.

Author Contributions: Conceptualization, Z.Z. and Q.S.; data curation, X.F.; methodology, X.F., S.W. and Y.F.; resources, Z.Z. and X.F.; validation, Q.S. and S.W.; writing—original draft, Z.Z. and Y.F.; corrections, modifications, and final acceptance, all authors. All authors have read and agreed to the published version of the manuscript.

Funding: This paper was funded by the Open Research Fund of the State Key Laboratory of Geohazard Prevention and Geo-environment Protection (Grant No. SKLGP2022K010), the Key R&D Program of Yunnan Province (202303AA080010), Natural Science Foundation joint funding of Liaoning (Grant No. 2023-BSBA-261), Basic Research Program of Liaoning Provincial Department of Education (Grant No. LJ212410142010), the Youth Innovation Promotion Association CAS (Grant No. 2021325), National Natural Science Foundation of China (Grant No. 52409137, 52179117).

Data Availability Statement: The original contributions presented in the study are included in the article; further inquiries can be directed to the corresponding author.

Acknowledgments: Thank you to all the authors who have contributed to the research in this field.

Conflicts of Interest: Author Yuwei Fang was employed by the company Yunnan Institute of Transport Planning and Design Co., Ltd. The remaining authors declare that the research was conducted in the absence of any commercial or financial relationships that could be construed as a potential conflict of interest.

Nomenclature

PDEM	Particle discrete element method
UCS	Uniaxial compression strength
Cc	Coefficient of curvature
Cu	Uniformity coefficient
D_{60}	Constrained grain size
D_{30}	Median grain size
D_{10}	Effective grain size
EI	Elongation index
FI	Flatness index
μ	Friction coefficient
$\sigma_{S\text{-}RM}$	UCS of soil–rock mixture with a certain rock content
σ_c	UCS of soil matrix
$\sigma_{S\text{-}RM}/\sigma_c$	Strength disturbance ratio

References

1. You, X. Stochastic structural model of the earth-rock aggregate and its application. *Chin. J. Rock Mech. Eng.* **2002**, *48*, 1748.
2. Xu, W.J.; Hu, R.L.; Tan, R.J. Some geomechanical properties of soil-rock mixtures in the Hutiao Gorge area, China. *Geotechnique* **2007**, *57*, 255–264. [CrossRef]
3. Zhang, Y.; Lu, J.Y.; Han, W.; Xiong, Y.W.; Qian, J.S. Effects of moisture and stone content on the shear strength characteristics of soil-rock mixture. *Materials* **2023**, *16*, 567. [CrossRef] [PubMed]
4. Deng, H.W.; Zhao, B.K.; Xiao, Y.G.; Tian, G.L. Experimental study on macroscopic mechanical characteristics and microscopic pore structure evolution of soil-rock mixture under repeated freeze-thaw cycles. *Appl. Sci.* **2023**, *13*, 11504. [CrossRef]
5. Wei, H.Z.; Wang, R.; Hu, M.J.; Zhao, H.i.; Xu, X.Y. Strength behaviour of gravelly soil with different coarse-grained contents in Jiangjiagou Ravine. *Rock Soil Mech.* **2008**, *29*, 48–51+57.
6. Tang, J.; Xu, D.; Liu, H. Effect of gravel content on shear behavior of sand-gravel mixture. *Rock Soil Mech.* **2018**, *39*, 93–102.
7. Zhang, Z.P.; Fu, X.D.; Sheng, Q.; Du, Y.X.; Zhou, Y.Q.; Huang, J.H. Stability of cracking deposit slope considering parameter deterioration subjected to rainfall. *Int. J. Geomech.* **2021**, *21*, 05021001. [CrossRef]
8. Yang, Y.T.; Chen, T.; Wu, W.; Zheng, H. Modelling the stability of a soil-rock-mixture slope based on the digital image technology and strength reduction numerical manifold method. *Eng. Anal. Bound. Elem.* **2021**, *126*, 45–54. [CrossRef]
9. Wei, G.; Javed, I.; Ruilin, H. Investigation of geomechanical characterization and size effect of soil-rock mixture: A case study. *Bull. Eng. Geol. Environ.* **2021**, *80*, 6263–6274. [CrossRef]
10. Zou, Y.X.; Zhang, J.M.; Wang, R. Seismic analysis of stone column improved liquefiable ground using a plasticity model for coarse-grained soil. *Comput. Geotech.* **2020**, *125*, 103690. [CrossRef]
11. Wang, T.; Yan, C.Z.; Zheng, Y.C.; Jiao, Y.Y.; Zou, J.P. Numerical study on the effect of meso-structure on hydraulic conductivity of soil-rock mixtures. *Comput. Geotech.* **2022**, *146*, 104726. [CrossRef]
12. An, N.; Wang, Q.N.; Feng, Y.Z.; Qin, Y.L.; Huang, L.K.; Tian, Y.Q.; Zhang, F.P.; Zhao, Z.H.; Chen, J.; Yao, C.R. Study on the impact of physical characteristics of soil-rock composite medium on its relative permittivity based on laboratory experiments. *Front. Earth Sci.* **2024**, *12*, 1342003. [CrossRef]
13. Xie, Y.; Yang, J.; Zheng, X.; Qu, T.; Zhang, C.; Fu, J. Effect of Particle Size Distributions (PSDs) on ground responses induced by tunnelling in dense coarse-grained soils: A DEM investigation. *Comput. Geotech.* **2023**, *163*, 105763. [CrossRef]
14. Wang, Y.; Li, X.; Li, S.; LI, G. Study on cracking characteristics of soil-rock mixture under uniaxial compression. *Chin. J. Rock Mech. Eng.* **2015**, *34*, 3541–3552.
15. Guo, Y.; Zhao, Y.; Feng, G.; Ran, H.; Zhang, Y. Study on damage size effect of cemented gangue backfill body under uniaxial compression. *Chin. J. Rock Mech. Eng.* **2021**, *40*, 2434–2444.
16. Hu, F.; Li, Z.; Sun, K.; Hu, R.L. Comparison of failure characteristics of frozen soil-stone mixture, ice-stone mixture and frozen soil under compression and tension. *Chin. J. Rock Mech. Eng.* **2021**, *40*, 2923–2934.

17. Afifipour, M.; Moarefvand, P. Mechanical behavior of bimrocks having high rock block proportion. *Int. J. Rock Mech. Min. Sci.* **2014**, *65*, 40–48. [CrossRef]
18. Lindquist, E.S. *The Strength and Deformation Properties of Melange*; University of California: Berkeley, CA, USA, 1994.
19. Altinsoy, H. A Physical Based Model Investigation for Determination of Shear Strength of Block in Matrix Rocks. Master's Thesis, Hacettepe University, Ankara, Türkiye, 2006; 91p.
20. Lei, X.Q.; Zhang, W.Y.; Chen, X.Q.; Ming, L. Influence of internal erosion on rainfall-induced instability of layered deposited-soil slopes. *Mathematics* **2023**, *11*, 4348. [CrossRef]
21. Li, J.; Li, L.W.; Li, S.C.; Jiang, L.F.; Chen, S.X.; Yu, F.; Dai, Z.J. Changes in the stability of a superhigh-deposit slope considering the influence of seepage erosion. *Int. J. Geomech.* **2024**, *24*, 04024119. [CrossRef]
22. Ren, Q. Stability analysis for coupling hydraulic-mechanical unsaturated deposit body under rainfall infiltration. In Proceedings of the 2nd Global Conference on Civil, Structural and Environmental Engineering (GCCSEE 2013), Shenzhen, China, 28–29 September 2013; pp. 768–772.
23. Zhong, Z.; Bie, C.; Lun, H.; YiLiang, T. Research on one-dimensional consolidation model of soil-rock mixtures backfill under Forchheimer seepage model. *Chin. J. Undergr. Space Eng.* **2019**, *15*, 473–480+488.
24. Liu, S.Q.; Wang, H.L.; Xu, W.Y.; Cheng, Z.C.; Xiang, Z.P.; Xie, W.C. Numerical Investigation of the Influence of Rock Characteristics on the Soil-Rock Mixture (SRM) Slopes Stability. *Ksce J. Civ. Eng.* **2020**, *24*, 3247–3256. [CrossRef]
25. He, J.X.; Fu, H.Y.; Zhang, Y.B.; Wan, A.L. The effect of surficial soil on the seismic response characteristics and failure pattern of step-like slopes. *Soil Dyn. Earthq. Eng.* **2022**, *161*, 107441. [CrossRef]
26. Chen, L.; Zhang, P.; Zheng, H. Mesostructure modeling of soil-rock mixtures and study of its mesostructural mechanics based on numerical manifold method. *Rock Soil Mech.* **2017**, *38*, 2402–2410.
27. Yang, Y.T.; Guo, H.W.; Fu, X.D.; Zheng, H. Boundary settings for the seismic dynamic response analysis of rock masses using the numerical manifold method. *Int. J. Numer. Anal. Methods Geomech.* **2018**, *42*, 1095–1122. [CrossRef]
28. Ye, Z.Y.; Xie, J.H.; Lu, R.L.; Wei, W.; Jiang, Q.H. Simulation of seismic dynamic response and post-failure behavior of jointed rock slope using explicit numerical manifold method. *Rock Mech. Rock Eng.* **2022**, *55*, 6921–6938. [CrossRef]
29. Shi, Z.M.; Zheng, H.C.; Yu, S.B.; Peng, M.; Jiang, T. Application of CFD-DEM to investigate seepage characteristics of landslide dam materials. *Comput. Geotech.* **2018**, *101*, 23–33. [CrossRef]
30. Xia, J.C.; Jing, L.; Chen, J.F.; Peng, M. Effects of slope topography on rock avalanche mobility and deposition: A 2-D discrete element method investigation. In Proceedings of the 5th GeoShanghai International Conference, Shanghai, China, 26–29 May 2024.
31. Zhang, H.; Lu, Y. Continuum and discrete element coupling approach to analyzing seismic responses of a slope covered by deposits. *J. Mt. Sci.* **2010**, *7*, 264–275. [CrossRef]
32. Savvides, A.A.; Papadrakakis, M. A computational study on the uncertainty quantification of failure of clays with a modified Cam-Clay yield criterion. *SN Appl. Sci.* **2021**, *3*, 659. [CrossRef]
33. Chwała, M. Undrained bearing capacity of spatially random soil for rectangular footings. *Soils Found.* **2019**, *59*, 1508–1521. [CrossRef]
34. Wang, C.; Chen, J.; Chen, L.L.; Sun, Y.; Xie, Z.L.; Yin, G.A.; Liu, M.H.; Li, A.Y. Experimental and modeling of residual deformation of soil-rock mixture under freeze-thaw cycles. *Appl. Sci.* **2022**, *12*, 8224. [CrossRef]
35. Zhang, M.; Liu, X.; Wang, P.; Du, L. Shear properties and failure meso-mechanism of soil-rock mixture composed of mudstone under different rock block proportions. *J. Civ. Environ. Eng.* **2019**, *41*, 17–26.
36. Wen, R.J.; Tan, C.; Wu, Y.; Wang, C. Grain size effect on the mechanical behavior of cohesionless coarse-grained soils with the discrete element method. *Adv. Civ. Eng.* **2018**, *2018*, 4608930. [CrossRef]
37. Medley, E.W. *The Engineering Characterization of Melanges and Similar Block-in-Matrix Rocks (Bimrocks)*; University of California: Berkeley, CA, USA, 1994.
38. *GB/T 50123-2019*; Standard for Geotechnical Testing Method. China Planning Press: Beijing, China, 2019.
39. *GB/T 50941-2014*; Standard for Terms Used in Building Foundation. China Architecture & Building Press: Beijing, China, 2014.
40. *JGJ/T 84-2015*; Standard for Terminology of Geotechnical Investigation. China Architecture & Building Press: Beijing, China, 2015.